

A first principle (3+1) dimensional model for microtubule polymerization

Vahid Rezania^{1,2} and Jack A. Tuszynski¹

1-Department of Physics, University of Alberta, Edmonton, AB T6G 2J1, Canada

2 - Department of Science, Grant MacEwan College, Edmonton, AB T5J 2P2, Canada

Abstract

In this paper we propose a microscopic model to study the polymerization of microtubules (MTs). Starting from fundamental reactions during MT's assembly and disassembly processes, we systematically derive a non-linear system of equations that determines the dynamics of microtubules in 3D. We found that the dynamics of a MT is mathematically expressed via a cubic-quintic nonlinear Schrödinger (NLS) equation. Interestingly, the generic 3D solution of the NLS equation exhibits linear growing and shortening in time as well as temporal fluctuations about a mean value which are qualitatively similar to the dynamic instability of MTs observed experimentally. By solving equations numerically, we have found spatio-temporal patterns consistent with experimental observations.

PACS numbers: 87.15.-v, 05.40.+j

I. INTRODUCTION

More than 25 years ago, Del Giudice et al. [1] argued that a quantum field theory approach to the collective behaviors of biological systems is not only applicable but the most adequate as it leads naturally to nonlinear, emergent behavior which is characteristic of biological organization. They followed a line of reasoning championed by Davydov [2, 3] and Fröhlich [4] who emphasized integration of both conservative and dissipative mechanisms in biological matter leading to the emergence of spatio-temporal coherence with various specific manifestations such as almost lossless energy transport and long-range coordination.

Microtubules (MTs) are long protein polymers present in almost all living cells. They participate in a host of cellular functions with great specificity and spatio-temporal organization. Microtubules are assembled by tubulin polymerization into a helical lattice forming a cylinder which is rigid and straight by biological standards. These protein polymers, typically several microns long, participate in fundamental cellular processes such as locomotion, morphogenesis, and reproduction [5]. It is also suggested that MTs are responsible for transferring mechanical energy across the cell, with little or no dissipation.

Both *in vivo* and *in vitro* observations confirmed that an individual microtubule switches stochastically between assembly and disassembly states making MTs highly dynamic structures [6]. This property of MTs is referred to as dynamic instability and it is a nonequilibrium process. It is generally believed that the instability starts from the hydrolysis of guanosine triphosphate (GTP) bound to tubulin converting it to guanosine diphosphate (GDP). This reaction is exothermic and releases $\sim 8kT$ energy per reaction [7], i.e. approximately 0.22 eV per molecule [8] at room temperature. Here k is the Boltzmann constant and T is the absolute temperature. Since GDP-bound tubulin favors dissociation, a MT enters the depolymerization phase as the advancing hydrolysis reaches the growing end of a MT. This dynamic phase transition is called a catastrophe. As a result, MTs rapidly disassemble releasing GDP-tubulin in the solution where reverse hydrolysis takes place followed by a re-polymerization phase of MTs called a rescue. Therefore, MTs constantly fluctuate between growth and shrinkage phases.

Several theoretical models have been proposed for a macroscopic description of these processes using nonlinear classical equations [9–20]. These phenomenological models provide good agreement with experiment but generally consider a MT as a one-dimensional mathematical object that switches stochastically between growth and shrinkage states. Even two-dimensional [9, 10, 19] and three-dimensional [20] considerations for MT polymerization have started from a given 2D (planar) or 3D (cylindrical) mathematical configuration that can grow or shrink randomly.

In this paper, however, we based our model on fundamental biochemical reactions that are occurring during microtubule's assembly and disassembly processes. This enables us to derive a nonlinear system

particular, our model explains the continuum symmetry breaking of an isotropic pool of tubulin dimers that leads to formation of experimentally observed 3D structures such as ring-shaped or filaments [21–23]. We believe that this treatment is necessary to address the fundamental issues about the observed dynamical behavior of MTs. As stated by Del Giudice et al. [1]: “Systems with collective modes are naturally described by field theories. Furthermore, quantum theory has proven to be the only successful tool for describing atoms, molecules and their interactions.”

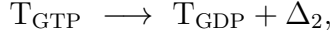
II. THE MODEL

Consider an individual MT in a free tubulin solution containing a large number of GTP-tubulin, GDP-tubulin and a pool of free GTP molecules. In this solution several processes take place (as well as their reverse reactions):

(i) GTP hydrolysis:



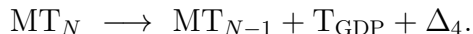
(ii) conversion of tubulin GDP from tubulin GTP:



(iii) growth of a MT:



(iv) shrinkage of a MT:



Experimental studies determined the free energy values for these reactions as: $\Delta_1 \simeq 220$ meV, $\Delta_2 \simeq 160$ meV and $\Delta_3 \simeq \Delta_4 \simeq 13 \times 40 = 420$ meV, respectively [24]. They are clearly above the thermal energy at room temperature ($kT \simeq 26$ meV) and within a quantum mechanical energy range that corresponds to the creation of one or a few chemical bonds. Hence we may consider each chemical reaction as a quantum mechanical process [25]. As a result, an individual microtubule with length L can be viewed as consisting of N tubulin layers defining its quantum state $|N\rangle$. A tubulin layer consists of at least one tubulin dimer and at most 13 tubulin dimers as observed in the MT’s structure. The state can be raised/lowered by a creation/annihilation operator (i.e. polymerization/depolymerization process) to the $|N+1\rangle/|N-1\rangle$ state. The corresponding MT is then longer/shorter by one tubulin layer compared to the original one.

Further simplification will be achieved by combining the above processes into two fundamental reactions:

(I) growth of a MT by one dimer length by adding of one tubulin layer in an endothermic process:

(II) shrinkage of a MT by one dimer length due to the removal of one layer of T_{GDP} dimers in an exothermic process:



where Δ is the energy of the reaction. In order to derive a quantum mechanical description of mechanisms (1) and (2), we introduce quantum states of a MT, tubulin and the heat bath, respectively:

- $|N\rangle$ is the state of a microtubule with N dimers (containing both GTP and GDP tubulins).
- $|N_T\rangle$ is the state of a tubulin dimer, T_{GTP} or T_{GDP} .
- $|\tilde{N}\rangle$ is the GTP hydrolysis energy state.

Then, the relevant second quantization operators would be:

$$\begin{aligned} a^\dagger &= |N+1\rangle\langle N|, & a &= |N-1\rangle\langle N|, \\ b^\dagger &= |N_T+1\rangle\langle N_T|, & b &= |N_T-1\rangle\langle N_T|, \\ d^\dagger &= |\tilde{N}+1\rangle\langle \tilde{N}|, & d &= |\tilde{N}-1\rangle\langle \tilde{N}|. \end{aligned} \quad (3)$$

Here b/b^\dagger and d/d^\dagger are annihilation/creation operators of tubulin and energy quanta, respectively. The operators a/a^\dagger are lowering/raising the number of tubulin layers in a MT. The creation and annihilation operators obey the Bose-Einstein commutation relations

$$[q_{\mathbf{k}}, q_{\mathbf{m}}^\dagger] = \delta_{\mathbf{k}\mathbf{m}}, \quad \text{and} \quad [q_{\mathbf{k}}^\dagger, q_{\mathbf{m}}^\dagger] = 0 = [q_{\mathbf{k}}, q_{\mathbf{m}}], \quad (4)$$

where $[A, B] = AB - BA$ is the Dirac commutator or $q = a, b$, and d . Following [26], one can express the above processes using creation and annihilation operators (3):

$$a^\dagger b d : \Delta + \text{MT}_{N-1} + T_{\text{GTP}} \longrightarrow \text{MT}_N \quad (5)$$

$$d^\dagger b^\dagger a : \text{MT}_N \longrightarrow \text{MT}_{N-1} + T_{\text{GDP}} + \Delta \quad (6)$$

Operators (5) and (6) describe a MT's growth and shrinkage by one layer, respectively. The polymerization or depolymerization process may happen repeatedly before reversing the process which can be captured by constructing product operators, i.e. $(a^\dagger b d)^m$ and $(d^\dagger b^\dagger a)^n$, where m and n are the number of growing or shrinking events in a sequence, respectively. Based on the mechanisms in (5) and (6), the Hamiltonian for interacting microtubules with $T_{\text{GTP}}/T_{\text{GDP}}$ tubulins can be written as

$$\begin{aligned} H &= \sum_{\mathbf{k}} \hbar\omega_{\mathbf{k}} a_{\mathbf{k}}^\dagger a_{\mathbf{k}} + \sum_{\mathbf{m}} \hbar\varpi_{\mathbf{m}} b_{\mathbf{m}}^\dagger b_{\mathbf{m}} + \sum_{\mathbf{l}} \hbar\sigma_{\mathbf{l}} d_{\mathbf{l}}^\dagger d_{\mathbf{l}} \\ &+ \sum_{\mathbf{k}}^{\infty} \sum_{\mathbf{m}} \hbar[\Gamma_{\tilde{\mathbf{k}}_n \tilde{\mathbf{m}}_n \tilde{\mathbf{l}}_n} c_{\tilde{\mathbf{k}}_n \tilde{\mathbf{m}}_n \tilde{\mathbf{l}}_n} + \Gamma_{\tilde{\mathbf{k}}_n \tilde{\mathbf{m}}_n \tilde{\mathbf{l}}_n}^* c_{\tilde{\mathbf{k}}_n \tilde{\mathbf{m}}_n \tilde{\mathbf{l}}_n}^\dagger], \end{aligned} \quad (7)$$

where ω , ϖ , σ and Γ are constants that can be related to the energy of the fundamental processes [27]. A growing/shrinking MT may change its state quickly or after several steps to a depolymerizing/polymerizing state and then may change back to a polymerizing/depolymerizing state. Experimentally, at a mesoscopic level the transition from the growing to the shrinking phase is quantified by the catastrophe rate f_{cat} and the transition from the shrinking to the growing phase is expressed by the rescue rate f_{res} in which $f_{\text{res}} < f_{\text{cat}}$. In the Hamiltonian (7), these transitions correspond to a combination of creation and annihilation operators as the n^{th} power of the reaction in (5) and (6):

$$c_{\tilde{\mathbf{k}}_n \tilde{\mathbf{m}}_n} = (a_{\mathbf{k}_1}^\dagger b_{\mathbf{m}_1} d_{\mathbf{l}_1})(a_{\mathbf{k}_2}^\dagger b_{\mathbf{m}_2} d_{\mathbf{l}_2}) \dots (a_{\mathbf{k}_n}^\dagger b_{\mathbf{m}_n} d_{\mathbf{l}_n}). \quad (8)$$

Here $\tilde{\mathbf{k}}_n = \{\mathbf{k}_1, \mathbf{k}_2, \dots, \mathbf{k}_n\}$ is a collection of indices and $\sum_{\tilde{\mathbf{k}}_n} = \sum_{\mathbf{k}_1} \sum_{\mathbf{k}_2} \dots \sum_{\mathbf{k}_n}$. We note that the momentum conservation for the last two terms in the Hamiltonian (7) requires that $\mathbf{l}_n = \sum_{i=1}^n \mathbf{k}_i - \sum_{i=1}^n \mathbf{m}_i - \sum_{i=1}^{n-1} \mathbf{l}_i$. Therefore, the first $n-1$ of \mathbf{l} will be free and summed in the Hamiltonian (7).

III. THE DYNAMICAL EQUATIONS

The Heisenberg equation of motion for a space- and time-dependent operator $q(\mathbf{r}, t)$ reads: $i\hbar\partial_t q(\mathbf{r}, t) = -[H, q(\mathbf{r}, t)]$, where H is the Hamiltonian. A system of coupled equations that describes the quantum dynamics of a MT can be derived from the Heisenberg equation. However, since MTs are overall classical objects (although some of their degrees of freedom may behave as quantum observables), we need to ensemble average over all possible states to obtain effective dynamical equations. Fourier transforming a_η , b_η and d_η operators over all states, we find

$$\psi(\mathbf{r}, t) = \Omega^{-1/2} \sum_{\eta} \exp(-i\eta \cdot \mathbf{r}) a_\eta(t), \quad (9)$$

$$\chi(\mathbf{r}, t) = \Omega^{-1/2} \sum_{\eta} \exp(-i\eta \cdot \mathbf{r}) b_\eta(t), \quad (10)$$

$$\phi(\mathbf{r}, t) = \Omega^{-1/2} \sum_{\eta} \exp(-i\eta \cdot \mathbf{r}) d_\eta(t), \quad (11)$$

where Ω is the volume over which the members of the plane wave basis are normalized [28, 29]. Here $\psi(\mathbf{r}, t)$, $\chi(\mathbf{r}, t)$, and $\phi(\mathbf{r}, t)$ are the corresponding field operators for the quantum operators a_η , b_η and d_η , respectively. The derivation of the equation of motion for the field operators is lengthy but straightforward and given in detail in [30]. The final form of the equations of motion is found to be

$$i\partial_t \psi + i\mathbf{v} \cdot \nabla \psi = -b\nabla^2 \psi + V\psi, \quad (12)$$

$$i\partial_t \chi = -e\nabla^2 \chi + U\chi, \quad (13)$$

$$V(|\psi|, |\chi|) = a + c|\chi|^4 |\psi|^2 - d|\chi|^6 |\psi|^4,$$

$$U(|\psi|) = f - h|\psi|^2,$$

TABLE I: The parameters available in the literature.

Parameter	Simulation Coeff.	Exp. Value	Reference
MT growth rate	Real(c)	0.50 – 19.7 ($\mu\text{m}/\text{min}$)	[31]
MT shortening rate	Real(d)	4.1 – 34.9 ($\mu\text{m}/\text{min}$)	[31]
MT catastrophe frequency		0.12 – 3.636 ($/\text{min}$)	[31]
MT diffusion constant	b	2.6 – 30.3 ($\mu\text{m}^2/\text{min}$)	[32]
Tubulin diffusion constant	e	300 – 480 ($\mu\text{m}^2/\text{min}$)	[33]

For simplicity we assumed that the energy in the system is distributed uniformly during the course of experiment. As a result, $\dot{\phi} = 0$ and $\nabla\phi = \mathbf{0}$. Here parameters a, b, e and f are real but c, d and h are complex. Table 1 lists experimental values for some of these parameters. Eq. (12) represents the nonlinear cubic-quintic Schrödinger (NLS) equation with a complex potential that has been extensively studied in connection with topics such as pattern formation, nonlinear optics, Bose-Einstein condensation, superfluidity and superconductivity, etc. [34]. A general solution of the NLS equation can be cast in the form of

$$\psi(\mathbf{r}, t) = R(\mathbf{r}, t) \exp[iS(\mathbf{r}, t)], \quad (14)$$

which involves topological defects (point in 2D and line in 3D). In 3D space these defects represent 1D strings or vortex filaments [34]. Furthermore, it is shown that the symmetry group of the cubic-quintic NLS equation is an extended Galilei group that includes translational and rotational symmetries as well as proper Galilei boosts and total mass conservation [35]. Adding any constraints such as boundary conditions to the equation, however, will cause a symmetry breaking in the system. As an example, in a cylindrical coordinate system, due to the rotational symmetry breaking, the general solution reduces to a stationary solution that represents a straight vortex filament with a twist:

$$\psi(r, \theta, z, t) = R(r) \exp[i(\omega t + n\theta + w(r) + k_z z)], \quad (15)$$

where ω is the spiral frequency, $R(r)$ is the amplitude, $w(r)$ is the spiral phase function and integer n is the winding number of the vortex [35, 36]. The axial wave number k_z characterizes the vortex's twist. In the case of the NLS equation, a family of vortices that move with a constant velocity is also a solution [36].

Further symmetry breaking would lead to different 3D structures such as double-wall, ring-shaped, sheet-like, C-shaped and S-shaped ribbons, and hoop structures as seen during tubulin polymerization experiments [21–23].

IV. NUMERICAL RESULTS

Equations (12) and (13) are solved numerically with a no-flux boundary condition. As an initial condition we chose a straight vortex filament perturbed by small noise (eg. thermal or environmental noise). In Fig. 1 we compare the observed data on the MT length as a function of time with our simulation results. The length of a vortex is defined as [36]:

$$L(t) = \int \Theta(\psi_0 - |\psi(\mathbf{r}, t)|) d^3r, \quad (16)$$

where $\Theta(x)$ is the step function and ψ_0 is a constant. In Figs. 1 and 2 we compare the observed data on the MT length as a function of time with our simulation results. Experimental panels in Figs. 1 and 2 represent the experimental data published by Rezania *et al.* [37]. Simulation panels show the numerical results of the normalized vortex length as a function of time for the given set of parameters.

To provide a simple yet accurate and powerful comparison between experimental and simulation results, we graph recursive maps for the data points. The advantage of the recursive maps is the introduction of regularity into the data sets that allows for a better choice of adjustable parameters due to noise reduction inherent in the separation of data into subsets corresponding to independent processes. In spite of being very simple, recursive maps of assembly and disassembly processes of individual MTs can successfully reproduce many of the key characteristic features. Consider first the following stochastic map as the simplest case that illustrates the approach taken:

$$\ell(t_n + 1) = r[\ell(t_n) + \delta], \quad (17)$$

where $\ell(t_n)$ is the length of a microtubule after n time steps, t_n . The parameter r is chosen to be a random number with the following two possibilities:

$$r = \begin{cases} 1 & \text{with probability } p \\ 0 & \text{with probability } 1 - p \end{cases}$$

In terms of the MT polymerization process, p is the probability that a given event will result in assembly while $1 - p$ is the probability of a complete catastrophe of the MT structure. The above simplified model, therefore, is governed by only two adjustable parameters: (a) the probability of complete catastrophe $1 - p$ which is constant and independent of the length or time elapsed and (b) the rate of polymerization which is proportional to the length increment δ over the unit of time chosen in the simulation. Thus, the coefficient δ divided by the time step $\Delta t (= t_{n+1} - t_n)$ gives the average growth velocity of an individual MT. Such information can be used to fine tune the simulation parameters. We note that the slope of the line in the simulation panels in Fig. 1 can be adjusted by varying the real parts of parameters c and d . The frequency of catastrophe events can also be changed

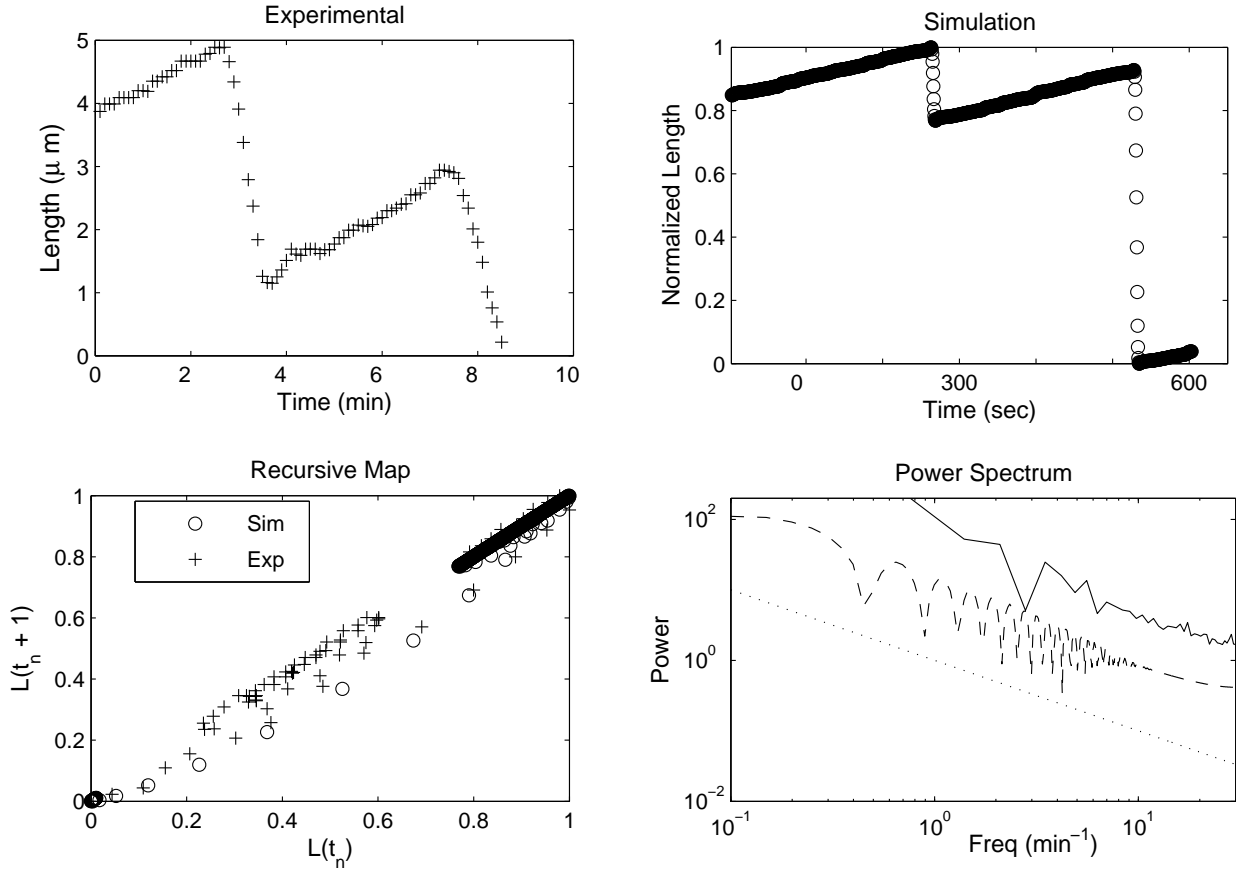


FIG. 1: Length of a distinct microtubule as a function of time. The top-left panel represent experimental data published in [37]. provided by O. Azarenko and M.A Jordan from the University of California, Santa Barbara. The top-right panel is the simulation result with the set of parameters ($a = 1, b = 10, c = 10 + i, d = 20 + i, e = 300, f = 1$ and $h = -.1 + i$). The bottom-left panel shows recursive maps for both experimental and simulation results. The bottom-right panel represents the power spectrum of the experimental (solid curve) and simulated (dashed curve) data, respectively. The curves are plotted at different offsets for clarity. No particular frequency of oscillation can be seen from the power spectrums. However, both power spectrums show a very similar broad distribution that more or less decays with frequency as an inverse power-law with slope ~ 1.0 . The best fit inverse power-law is shown by a dotted line.

map for both the experimental data and the simulation results. Based on the recursive maps, the key characteristics of the experimental and simulated results that were obtained independently are quite similar. This represents Eqs. (12) and truly describes the dynamics of MTs' polymerization.

To provide a more solid comparison, a spectral analysis is also carried on both experimental and simulated data. As discussed by Odde *et al.* [38], the power spectrum analysis is a more general way to characterize the microtubule assembly/disassembly dynamics without assuming any model *a priori*. The power spectrum panels in Figs. 1 and 2 represent the spectral power of the experimental and simulated data, respectively. As shown, there is a great agreement between the experimental (solid

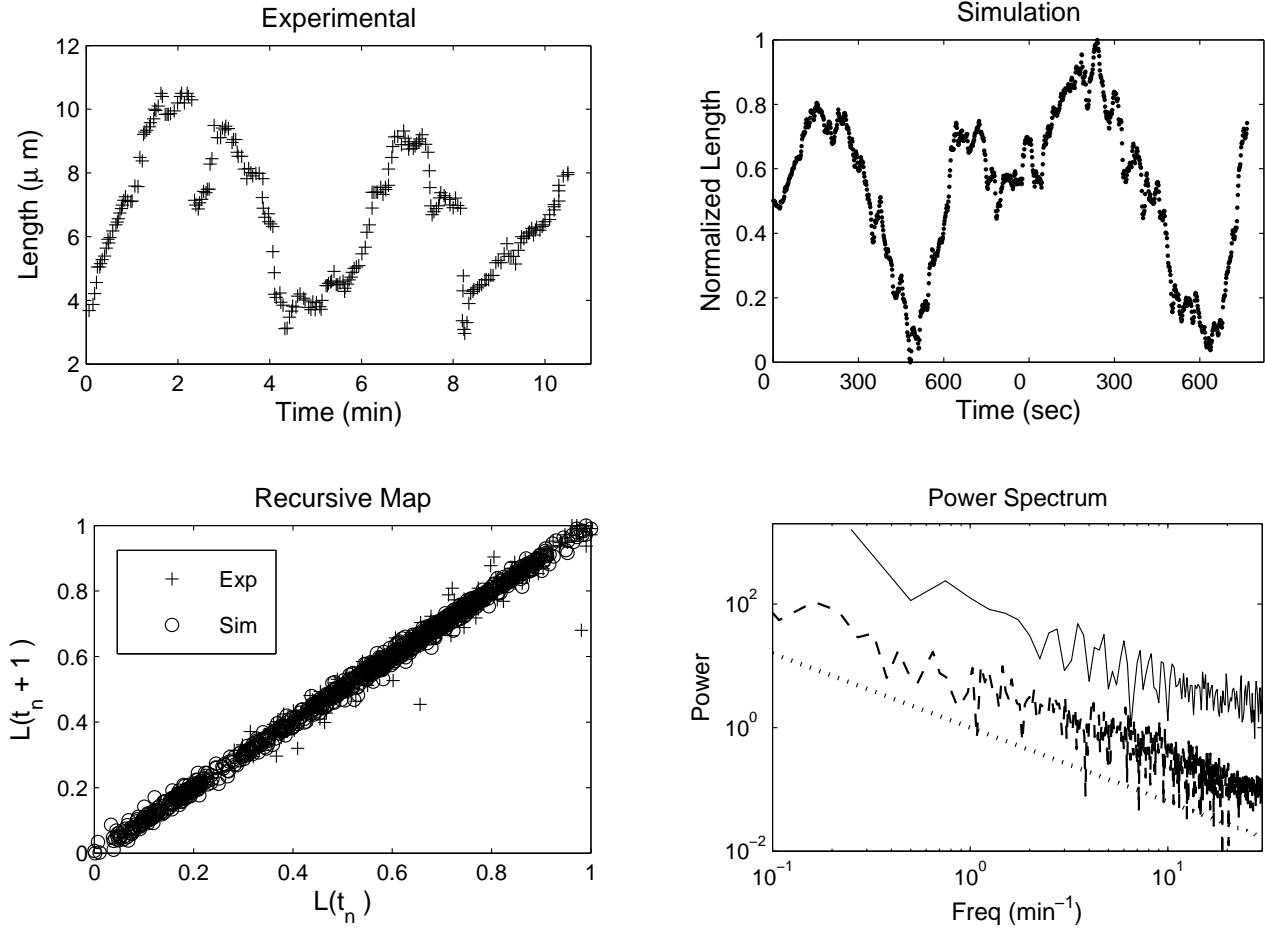


FIG. 2: Same as Fig 1. but with the set of parameters ($a = 1, b = 30, c = 10 + 10i, d = 20 + 10i, e = 300, f = 1$ and $h = -.1 + i$). In the power spectrum panel, the inverse power-law has a slope of ~ 1.2 .

curve) and simulated (dashed curve) spectrums. We note that the curves are plotted at different offsets for visual clarity only. As expected, no particular frequency of oscillation can be found from the power spectrums. However, both power spectrums demonstrate a very similar broad distribution that more or less decays with frequency as an inverse power-law with slope ~ 1.0 in Fig. 1 and ~ 1.2 in Fig. 2, respectively. The best fit inverse power-law is shown by a dotted line in both panels.

Although this is not unique to the model presented here, our results show no attenuation states during MT polymerization (Figs. 1 and 2). The MT length undergoes small fluctuations all the time. This can be understood by noting that our model is based on the cyclic polymerization and depolymerization of tubulin dimers. Behavior consistent with this result has recently been observed by Schek *et al.*[39] who studied the microtubule assembly dynamics at higher spatial ($\sim 1\text{-}5$ nm) and temporal (~ 5 kHz) resolutions. They found that even in the growth phase, a MT undergoes shortening excursions at the nanometer scale

V. DISCUSSION

The basic structural unit of a MT is the tubulin dimer. Each dimer exists in a quantum mechanical state characterized by several variables, especially GTP/GDP. Each microstate of a tubulin dimer is sensitive to the states of its neighbors. Tubulin dimers have both discrete degrees of freedom (distribution of charge) and continuous degrees of freedom (orientation). A model that focuses on the discrete variables will be an array of coupled binary switches [40], while a model that focuses on the continuous ones could be an array of coupled oscillators [41, 42]. Here we have focused on tubulin binding and GTP hydrolysis as the key biochemical processes determining the states of MTs which are most easily accessible to experimental determination. We have shown how a quantum mechanical description of the energy binding reactions taking place during MT polymerization can lead to nonlinear field dynamics with very rich behavior that includes both localized energy transfer and oscillatory solutions.

Based on the chemical binding reactions occurring during MT polymerization, a quantum mechanical Hamiltonian for the system has been proposed in this work. Equations of motion have then been derived and transformed from the purely quantum mechanical description to a semi-classical picture using the method of coherent structures. We found that the dynamics of a MT can be explained by the cubic-quintic nonlinear Schrödinger equation (NLS) with a complex potential. A generic solution of the NLS equation in cylindrical geometry is a vortex filament [34–36] which can grow or shrink linearly in time as well as fluctuate temporally with some frequency. This behavior exhibits two distinct dynamical phases: (a) linear growth/shrinkage and (b) oscillation about a mean value, which are indeed main experimentally observed characteristics of the MT dynamics (Fig. 1 and 2).

We have demonstrated here that the assembly process can be described starting from quantum mechanical first principles applied to biochemical reactions. This can be subsequently transformed into a highly nonlinear semi-classical dynamics problem. The gross features of MT dynamics satisfy classical field equations in a coarse-grained picture. Individual chemical reactions involving the constituent molecules still retain their quantum character. The method of coherent structures allows for a simultaneous classical representation of the field variables and a quantum approach to their fluctuations. Here, the overall MT structure (and their ensembles) can be viewed as a virtual classical object in (3+1)-D space-time. However, at the fundamental level of its constituent biomolecules, it is quantized as are chemical reactions involving its assembly or disassembly. In our approach the route taken is opposite since we started with individual tubulin quantum microstates to arrive at classical, nonlinear but classically coherent (and stable) macro-states of a microtubule.

Finally, we note that dynamics of pattern formation can be also described by NLS equation in which

al. [43] demonstrated that gravity can influence tubulin assembly reactions with MTs forming distinct bands at right angles to the orientation of the gravity field or, if spun, to the centrifugal force. Despite several studies [44–47], the above experiments are yet to be fully explained theoretically. Our goal in future studies is to focus on the dynamics of pattern formation by MTs using the results presented in this paper.

Acknowledgment This research was supported in part by the Natural Sciences and Engineering Research Council of Canada (NSERC) and the Canadian Space Agency (CSA). Insightful discussions with S. R. Hameroff and J. M. Dixon are gratefully acknowledged. The authors would also thank M. A. Jordan for providing microtubule assembly data. VR specially thanks I. Aranson for sharing his CGLE code and for fruitful discussions.

References

- [1] E. Del Giudice, S. Doglia, M. Milani, G. Vitiello, Nuclear Physics B251 (1985) 375.
- [2] A.S. Davydov, Biology and quantum mechanics (Pergamon, Oxford, 1982).
- [3] A.S. Davydov, Phys. Scripta 20 (1979) 387.
- [4] [3] H. Fröhlich, Rivista del Nuovo Cim. 7 (1977) 399; Advances in Electronics and Electron Physics, ed. L. Marion and C. Matron, vol. 53 (1980) p. 85.
- [5] B. Alberts *et al.* *Molecular Biology of the Cell* (Garland, New York, 1994).
- [6] T. Mitchison, M. Krischner, Nature (London) 312 (1984) 232; 312 (1984) 237.
- [7] R. A. Walker, S. A. Inoué, E. D. Salmon, J. Cell. Biol. 108 (1989) 931.
- [8] R. Audenaert, Y. Engelborghs, L. Heremans, K. Heremans, Biochim. Biophys. Acta 996 (1989) 110.
- [9] T. L. Hill, M. W. Kirschner, Int. Rev. Cytol. 78 (1982) 1.
- [10] P.M. Bayley, M. J. Schilstra, S. R. Martin, J Cell Sci. 95 (1990) 33.
- [11] M. Dogterom, S. Leibler, Phys. Rev. Lett. 70 (1993) 1347.
- [12] D. K. Fygenson, E. Braun, A. Libchaber, Phys. Rev. E 50 (1994) 1579.
- [13] M. Dogterom, A. C. Maggs and S. Leibler Proc. Natl. Acad. Sci. USA **92**, 6683 (1995).
- [14] B. Houchmandzadeh, M. Vallade, Phys. Rev. E 53 (1996) 6320.
- [15] E. Jobs, D. E. Wolf, H. Flyvbjerg, Phys. Rev. Lett. 79 (1997) 519.
- [16] M. Dogterom, B. Yurke, Phys. Rev. Lett. 81 (1998) 485.
- [17] D. J. Bicout, R. J. Rubin, Phys. Rev. E 59 (1999) 913.

- [19] V. VanBuren, D. J. Odde, L. Cassimeris, *Proc. Natl. Acad. Sci. U S A.* 99 (2002) 6035.
- [20] V. VanBuren, L. Cassimeris, D. J. Odde, *Biophys. J.* 89 (2005) 2911.
- [21] E. Unger, K. J. Bohm, W. Vater, *Electron Microsc. Rev.* 3 (1990) 355.
- [22] S. Behrens, W. Habicht, J. Wu, E. Unger, *Surface and Interface Analysis* 38 (2006) 1014.
- [23] W. Habicht, S. Behrens, E. Unger, E. Dinjus, *Surface and Interface Analysis* 38 (2006) 194.
- [24] M. Caplow, R. L. Ruhlen, J. Shanks, *J. Cell Biol.* 127 (1994) 779.
- [25] We note that GTP hydrolysis is a subtle biochemical process that carries a quantum of biological energy and thus allows us to make a link between quantum mechanics and polymer dynamics.
- [26] J. A. Tuszynski, J. M. Dixon, *Physica A* 290 (2001) 69.
- [27] J. M. Dixon, J. A. Tuszynski, P. L. Clarkson, (Oxford University Press, Oxford, 1997).
- [28] J. M. Dixon, J. A. Tuszynski, *Int. J. Mod. Phys. B* 9 (1995) 1611.
- [29] J. A. Tuszynski, J. M. Dixon, *J. Phys. A* 22 (1989) 4877.
- [30] V. Rezania, J. A. Tuszynski, *Physica. A.* 387 (2008) 5795.
- [31] S. Pedigo, R. C. Williams Jr., *Biophys. J.* 83 (2002) 1809.
- [32] I. V. Maly, *Bulletin Math. Biol.* 64 (2002) 213.
- [33] D. J. Odde, *Biophys. J.* 73 (1997) 88.
- [34] I. S. Aranson, L. Kramer, *Rev. Mod. Phys.* 74 (2002) 99.
- [35] L. Gagnon, P. Winternitz, *Phys. Rev. A* 39 (1989) 296.
- [36] I. S. Aranson, A. R. Bishop, *Phys. Rev. Lett.* 79 (1997) 4174.
- [37] V. Rezania, O. Azarenko, M. A. Jordan, H. Bolterauer, R. F. Luduea, J. T. Huzil, J. A. Tuszynski, *Biophys. J.* 95 (2008) 1993.
- [38] D. J. Odde, H. Buettner, L. Cassimeris, *AIChE J.* 42 (1996) 1434.
- [39] H. T. Schek, M. K. Gardner, J. Cheng, D. J. Odde, A. J. Hunt, *Current Biology* 17 (2007) 1445.
- [40] S. Rasmussen, H. Karampurwala, R. Vaidyanath, K. S. Hensen, S. R. Hameroff, *Physica D* 42 (1990) 428.
- [41] A. Samsonovich, A. Scott, S. R. Hameroff, *Nanobiology* 1 (1992) 457.
- [42] J. A. Brown, J. A. Tuszynski, *Phys. Rev. E* 56 (1997) 5834.
- [43] J. Tabony, D. Job, *Nature* 346 (1990) 448.
- [44] S. Portet, J. A. Tuszynski, J. M. Dixon, M. V. Sataric, *Stat. Nonlin Soft Matter Phys.* 68 (2003) 021903.
- [45] J. A. Tuszynski, M. V. Sataric, S. Portet, J. M. Dixon, *Phys. Letts. A* 340 (2005) 175.
- [46] I. S. Aranson, L. S. Tsimring, *Phys. Rev. E* 71 (2005) 050901.
- [47] I. S. Aranson, L. S. Tsimring, *Phys. Rev. E* 74 (2006) 031915.